

- S. Olsen, and L. Pondrum, Phys. Rev. D **6**, 1254 (1972).
- ⁶C. Ankenbrandt, R. Larsen, L. Leipuner, L. Smith, F. Shively, R. Stefanski, R. Adair, H. Kasha, S. Merlan, R. Turner, and P. Wanderer, Phys. Rev. Lett. **28**, 1472 (1972).
- ⁷J. Sandweiss, J. Sunderland, W. Turner, W. Willis, and L. Keller, Phys. Rev. Lett. **30**, 1002 (1973).
- ⁸B. P. Roe, D. Sinclair, and J. C. VanderVelde, in *Proceedings of the Twelfth International Conference on High Energy Physics, Dubna, 1964*, edited by Ya. A. Smorodinskii *et al.* (Atomizdat, Moscow, 1966), Vol. 2, p. 478.
- ⁹Particle Data Group, Rev. Mod. Phys. **45**, S1 (1973).
- ¹⁰S. L. Maratek and S. P. Rosen, Phys. Lett. **29B**, 497 (1969).
- ¹¹D. Haidt *et al.* (X2 Collaboration), Phys. Rev. Lett. **29B**, 691 (1969).

Further measurements of forward-charged-pion electroproduction at large k^2 *

C. J. Bebek, C. N. Brown, M. Herzlinger, S. Holmes, C. A. Lichtenstein, F. M. Pipkin, and L. K. Sistrerone
Cyclotron Laboratory, Harvard University, Cambridge, Massachusetts 02138

D. Andrews,† K. Berkelman, D. G. Cassel, and D. L. Hartill
Laboratory of Nuclear Studies, Cornell University, Ithaca, New York 14850
 (Received 23 October 1973)

Measurements of the electroproduction reaction $e^- + p \rightarrow e^- + \pi^+ + n$ carried out at the Wilson Synchrotron Laboratory are reported. For fixed virtual photon-hadron center-of-mass energy, $W = 2.67$ GeV, data are presented with the mass of the virtual photon, $-k^2$, centered at 0.6, 1.2, and 2.0 GeV². At the central $-k^2 = 1.2$ (GeV²) point, results are also given for $W = 2.15$ GeV. For the $W = 2.67$, $-k^2 = 1.2$ GeV² setting, an angular scan is presented and the longitudinal transverse-interference term is extracted. The data are compared with an electric Born-model calculation of Berends which has as its only free parameter the pion electromagnetic form factor. The theory is used to extract new results for the pion form factor up to $-k^2 = 2.0$ GeV².

I. INTRODUCTION

In recent years the pion electroproduction reaction

$$e^- + p \rightarrow e^- + \pi^+ + n \quad (1)$$

has been studied intensively.¹⁻⁴ This reaction has generated interest for two closely related reasons. First, it has been observed that for small momentum transfer, the electric Born model gives a more than adequate description of reaction (1) and of the equivalent photoproduction reaction⁵

$$\gamma + p \rightarrow \pi^+ + n. \quad (2)$$

Second, if as suggested by the success of the electric Born model the dominant contribution is due to one-pion exchange, reaction (1) gives a direct measure of the pion electromagnetic form factor in the spacelike region.⁶

In this paper we present new measurements of pion electroproduction at higher values of $-k^2$ (the square of the mass of the virtual photon) and of W (the total center-of-mass energy of the virtual photon-proton system). Measurements were also

made at the same k^2 and different W so as to study the dependence on the minimum momentum transfer. The measurements are compared with the predictions of the electric Born model and found to be in good agreement for small momentum transfer. The data at zero degrees are used to determine the pion form factor for $-k^2$ up to 2 GeV².

These measurements represent a continuation of similar measurements at lower energies by some members of the group. Hence, we will rely on the previous report (Ref. 2) to supply the background for the kinematics, phenomenology, and theoretical ideas needed in applying the electric Born model to our results.

II. EXPERIMENT

This experiment was performed at the Wilson Electron Synchrotron. Figure 1 gives a schematic view of the apparatus. A beam of 9.6-GeV electrons was incident on a 12.7-cm-long liquid hydrogen target. An inelastically scattered electron was detected in the Cornell 10-GeV spectrometer. A

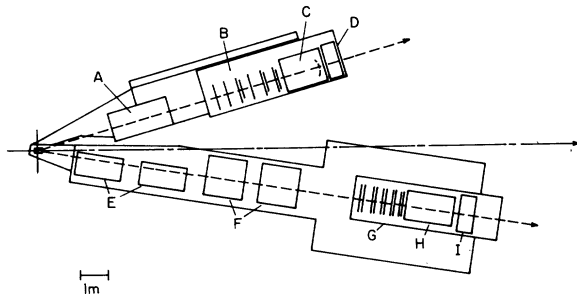


FIG. 1. A schematic diagram of the apparatus: A, 20D84 bending magnet; B, wire spark-chamber planes; C, Freon Čerenkov counter; D, shower counter; E, 8Q48 half quadrupole magnets; F, 18D36 bending magnets; G, proportional wire chambers; H, Freon counter; I, lead acetate shower counter.

Freon-gas Čerenkov counter and a heavy-liquid shower counter were used to identify the scattered electron, and a Freon-gas Čerenkov counter identified the scattered pion.

The electron spectrometer had a momentum acceptance of $\pm 20\%$ and an angular acceptance of $\pm \frac{1}{2}^\circ$ horizontally and $\pm 1^\circ$ vertically. The large momentum acceptance led to a spectrum of virtual photons with a high correlation in angle, W , ϵ (the polarization parameter), and to a lesser extent $-k^2$.

The hadron spectrometer had a momentum acceptance of $\pm 50\%$ and an angular aperture of $\pm 1^\circ$ horizontally and -2° to $+5^\circ$ vertically. By studying the mass spectrum of events which did not fire the Čerenkov counter, the efficiency of this counter for pions from reaction (1) was determined to be greater than 99%. The relative timing of the coincident pion and electron was measured with a rms resolution of 400 psec leading to a final cor-

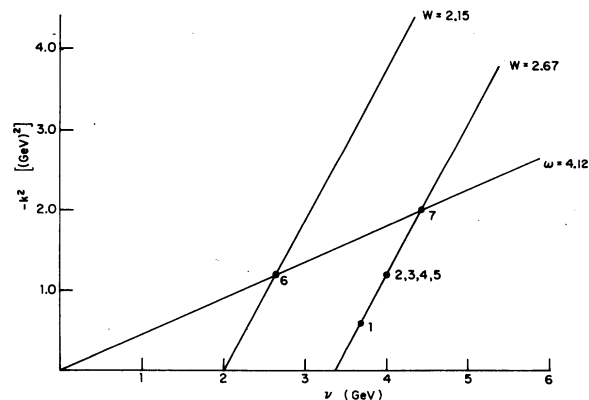


FIG. 2. A diagram showing the nominal values of $-k^2$ and W at which data were taken.

rection due to arm-to-arm randoms of less than 5%.

Setting the electron spectrometer at a certain angle and energy determined the nominal value of the mass $-k^2$ of the virtual photon and the total energy W of the final state. Figure 2 indicates the nominal values of these variables for which data were taken. For data points 1, 3, 6, and 7 the hadron spectrometer was set exactly along the nominal virtual-photon direction. Data point 2 had the hadron arm 3° toward the beam ($\phi = 0^\circ$) from the virtual-photon direction and data points 4 and 5 had the hadron arm 3° and 7° , respectively, outside the virtual-photon direction ($\phi = 180^\circ$). We thus obtained data for varying $-k^2$ at fixed $W = 2.67$ GeV and also data at varying W for fixed $-k^2 = 1.2$ GeV².

By combining the known beam momentum with the measured momenta of the detected electron and pion, the mass of the missing particles was calculated. Figure 3 shows a missing-mass-squared plot of the events obtained with the electron-arm nominal settings $W = 2.15$ GeV and $-k^2 = 1.20$ GeV². A large signal from reaction (1) is evident. All events within the cuts shown were then constrained by adjusting the scattered electron and pion momenta equally to give the known neutron mass. These events were then binned in the variables θ , the polar angle of the emitted pion in the center-of-mass system of the virtual-photon-production reaction, and ϕ , the angle between the plane determined by the virtual-photon-production reaction and the electron scattering plane. The bins had a typical full width at half maximum (FWHM) of 0.12 GeV in W , 0.12 GeV² in $-k^2$, and 0.02 in ϵ .

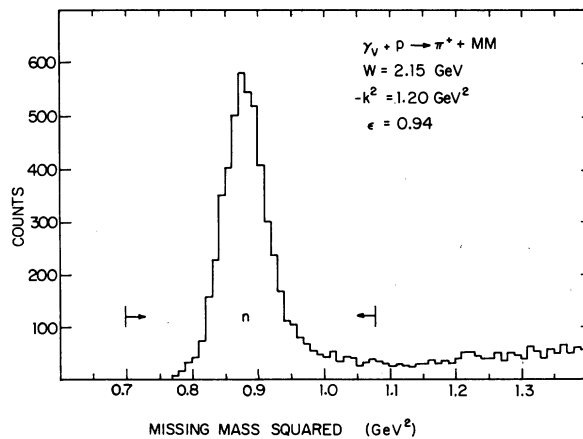


FIG. 3. A missing-mass-squared plot for the data point with nominal setting $W = 2.15$ GeV and $-k^2 = 1.20$ GeV².

TABLE I. The bins and the center-of-mass virtual-photoproduction cross sections for the reaction $\gamma^* + p \rightarrow \pi^+ + n$. The uncertainties are statistical only. N is the number of events in the bin.

Bin		Kinematic averages							Result	
ϕ (deg)	θ (deg)	θ (deg)	W (GeV)	$-k^2$ (GeV ²)	ϵ	$\cos\phi$	$\cos 2\phi$	$-t$ (GeV ²)	N	$\frac{d\sigma}{d\Omega_\pi} \left(\frac{\mu\text{b}}{\text{sr}} \right)$
(a) Data point 1										
all	≤ 1.5	1.063	2.674	0.621	0.866	0.094	-0.102	0.009	160	5.35 ± 0.50
-135 to -45	1.5 to 3.0	2.280	2.669	0.619	0.867	0.120	-0.678	0.011	95	5.07 ± 0.62
	3.0 to 4.5	3.767	2.666	0.615	0.868	0.115	-0.580	0.015	140	5.54 ± 0.56
	4.5 to 6.0	5.262	2.658	0.621	0.869	0.130	-0.551	0.022	120	5.07 ± 0.54
	6.0 to 7.5	6.660	2.646	0.617	0.872	0.181	-0.628	0.029	89	4.26 ± 0.52
	7.5 to 9.0	8.140	2.600	0.632	0.881	0.345	-0.540	0.039	41	3.68 ± 0.67
-45 to 45	1.5 to 3.0	2.343	2.618	0.631	0.879	0.909	0.665	0.012	130	5.33 ± 0.56
	3.0 to 4.5	3.823	2.579	0.645	0.886	0.903	0.646	0.017	230	5.87 ± 0.47
	4.5 to 6.0	5.248	2.541	0.652	0.893	0.907	0.660	0.023	340	7.69 ± 0.54
	6.0 to 7.5	6.779	2.509	0.664	0.898	0.899	0.632	0.031	310	5.54 ± 0.38
	7.5 to 9.0	8.238	2.478	0.679	0.903	0.907	0.660	0.041	310	5.56 ± 0.39
	9.0 to 10.5	9.694	2.451	0.683	0.908	0.897	0.627	0.051	260	5.34 ± 0.40
	10.5 to 12.0	11.215	2.417	0.699	0.913	0.908	0.664	0.063	170	4.46 ± 0.41
	12.0 to 13.5	12.649	2.390	0.715	0.917	0.914	0.685	0.076	110	4.51 ± 0.52
	13.5 to 15.0	14.162	2.344	0.720	0.923	0.935	0.758	0.090	59	3.26 ± 0.48
15.0 to 16.5	15.591	2.347	0.729	0.922	0.913	0.682	0.106	28	3.67 ± 0.78	
45 to 135	1.5 to 3.0	2.369	2.674	0.618	0.867	0.049	-0.669	0.011	110	5.19 ± 0.58
	3.0 to 4.5	3.813	2.668	0.616	0.867	0.065	-0.633	0.015	190	5.15 ± 0.44
	4.5 to 6.0	5.321	2.662	0.622	0.868	0.107	-0.632	0.022	290	5.06 ± 0.36
	6.0 to 7.5	6.774	2.667	0.618	0.867	0.062	-0.634	0.030	330	4.71 ± 0.31
	7.5 to 9.0	8.275	2.666	0.621	0.867	0.067	-0.644	0.041	400	4.96 ± 0.30
	9.0 to 10.5	9.696	2.681	0.616	0.863	0.031	-0.638	0.053	330	3.71 ± 0.23
	10.5 to 12.0	11.243	2.677	0.613	0.864	0.034	-0.707	0.068	250	2.86 ± 0.20
	12.0 to 13.5	12.673	2.691	0.616	0.860	0.040	-0.702	0.085	190	2.36 ± 0.19
	13.5 to 15.0	14.177	2.727	0.609	0.851	-0.038	-0.679	0.106	110	2.01 ± 0.20
	15.0 to 16.5	15.735	2.778	0.587	0.838	-0.115	-0.716	0.133	63	1.70 ± 0.23
16.5 to 18.0	17.154	2.889	0.548	0.811	-0.309	-0.711	0.167	33	1.69 ± 0.31	
135 to 225	1.5 to 3.0	2.327	2.740	0.603	0.852	-0.891	0.603	0.010	88	4.62 ± 0.57
	3.0 to 4.5	3.766	2.774	0.585	0.843	-0.918	0.702	0.014	100	2.70 ± 0.29
	4.5 to 6.0	5.253	2.802	0.574	0.836	-0.888	0.594	0.020	120	2.76 ± 0.28
	6.0 to 7.5	6.793	2.847	0.561	0.824	-0.880	0.562	0.030	110	2.57 ± 0.26
	7.5 to 9.0	8.104	2.873	0.553	0.817	-0.880	0.562	0.041	78	2.12 ± 0.26
	9.0 to 10.5	9.706	2.903	0.536	0.808	-0.826	0.380	0.057	36	1.39 ± 0.24
10.5 to 12.0	11.156	2.944	0.528	0.796	-0.844	0.435	0.076	25	2.10 ± 0.44	
(b) Data point 2										
all	≤ 1.5	0.979	2.904	1.068	0.806	0.301	-0.214	0.017	39	3.31 ± 0.56
-45 to 45	1.5 to 3.0	2.305	2.866	1.088	0.816	0.905	0.653	0.021	54	4.62 ± 0.69
	3.0 to 4.5	3.773	2.841	1.110	0.821	0.902	0.644	0.027	82	3.47 ± 0.41
	4.5 to 6.0	5.219	2.801	1.121	0.831	0.913	0.681	0.036	100	3.17 ± 0.35
	6.0 to 7.5	6.727	2.770	1.142	0.838	0.911	0.673	0.047	140	3.52 ± 0.33
	7.5 to 9.0	8.122	2.728	1.157	0.847	0.904	0.649	0.059	98	2.05 ± 0.22
	9.0 to 10.5	9.750	2.690	1.182	0.856	0.927	0.733	0.076	120	2.19 ± 0.21
	10.5 to 12.0	11.266	2.661	1.199	0.861	0.903	0.646	0.093	130	2.31 ± 0.21
	12.0 to 13.5	12.743	2.620	1.217	0.869	0.928	0.735	0.111	100	1.53 ± 0.16
	13.5 to 15.0	14.152	2.583	1.223	0.876	0.927	0.734	0.129	99	1.47 ± 0.16
	15.0 to 16.5	15.696	2.563	1.253	0.879	0.911	0.673	0.152	100	1.41 ± 0.15
	16.5 to 18.0	17.231	2.524	1.285	0.885	0.923	0.715	0.176	63	0.87 ± 0.11
	18.0 to 19.5	18.664	2.506	1.277	0.888	0.915	0.689	0.198	59	0.85 ± 0.12
	19.5 to 21.0	20.237	2.458	1.318	0.895	0.941	0.782	0.224	40	0.73 ± 0.12
	21.0 to 22.5	21.621	2.443	1.328	0.897	0.935	0.759	0.249	19	0.51 ± 0.12
	22.5 to 24.0	23.038	2.428	1.328	0.899	0.916	0.685	0.274	20	0.91 ± 0.20

TABLE I (Continued)

Bin		Kinematic averages							Result	
ϕ (deg)	θ (deg)	θ (deg)	W (GeV)	$-k^2$ (GeV ²)	ϵ	$\cos\phi$	$\cos 2\phi$	$-t$ (GeV ²)	N	$\frac{d\sigma}{d\Omega_\pi} \left(\frac{\mu\text{b}}{\text{sr}} \right)$
(b) Data point 2										
45 to 135	1.5 to 3.0	2.361	2.912	1.053	0.804	0.047	-0.652	0.019	46	3.70 ± 0.60
	3.0 to 4.5	3.814	2.914	1.059	0.803	0.194	-0.650	0.025	77	3.70 ± 0.45
	4.5 to 6.0	5.315	2.898	1.072	0.806	0.174	-0.640	0.034	79	2.76 ± 0.33
	6.0 to 7.5	6.785	2.884	1.073	0.810	0.266	-0.627	0.044	94	2.64 ± 0.28
	7.5 to 9.0	8.178	2.869	1.079	0.814	0.241	-0.672	0.057	84	1.96 ± 0.23
	9.0 to 10.5	9.718	2.870	1.080	0.814	0.251	-0.749	0.073	88	1.95 ± 0.22
	10.5 to 12.0	11.295	2.850	1.094	0.818	0.282	-0.694	0.092	96	1.93 ± 0.20
	12.0 to 13.5	12.693	2.820	1.115	0.826	0.328	-0.659	0.112	75	1.38 ± 0.17
	13.5 to 15.0	14.194	2.831	1.112	0.822	0.282	-0.684	0.135	80	1.52 ± 0.18
	15.0 to 16.5	15.683	2.823	1.120	0.824	0.280	-0.695	0.160	46	1.10 ± 0.17
16.5 to 18.0	17.234	2.797	1.134	0.829	0.365	-0.587	0.188	40	1.25 ± 0.21	
(c) Data point 3										
all	≤1.5	0.997	2.657	1.205	0.862	-0.034	-0.019	0.029	99	4.32 ± 0.50
-135 to -45	1.5 to 3.0	2.371	2.654	1.209	0.863	0.031	0.608	0.032	47	3.30 ± 0.56
	3.0 to 4.5	3.681	2.657	1.207	0.862	0.024	-0.576	0.035	67	3.46 ± 0.46
	4.5 to 6.0	5.284	2.657	1.211	0.861	0.124	-0.567	0.044	64	2.83 ± 0.41
	6.0 to 7.5	6.610	2.648	1.195	0.863	0.013	-0.648	0.051	59	3.87 ± 0.56
	7.5 to 9.0	8.144	2.610	1.212	0.871	0.235	-0.545	0.064	24	2.07 ± 0.44
-45 to 45	1.5 to 3.0	2.311	2.606	1.230	0.871	0.890	0.597	0.035	59	3.67 ± 0.53
	3.0 to 4.5	3.837	2.578	1.245	0.876	0.896	0.662	0.041	110	4.36 ± 0.46
	4.5 to 6.0	5.325	2.547	1.251	0.882	0.902	0.642	0.049	120	3.08 ± 0.30
	6.0 to 7.5	6.742	2.518	1.269	0.887	0.903	0.647	0.060	140	3.19 ± 0.30
	7.5 to 9.0	8.257	2.490	1.286	0.891	0.903	0.648	0.072	150	2.98 ± 0.26
	9.0 to 10.5	9.730	2.466	1.302	0.894	0.916	0.690	0.086	140	2.89 ± 0.26
	10.5 to 12.0	11.129	2.442	1.320	0.897	0.901	0.639	0.101	89	2.07 ± 0.23
	12.0 to 13.5	12.667	2.410	1.328	0.902	0.905	0.657	0.118	71	2.32 ± 0.29
	13.5 to 15.0	14.252	2.393	1.333	0.905	0.869	0.533	0.136	44	1.91 ± 0.30
	15.0 to 16.5	15.494	2.368	1.361	0.908	0.896	0.622	0.153	22	1.40 ± 0.30
16.5 to 18.0	17.117	2.355	1.358	0.909	0.861	0.495	0.176	25	2.24 ± 0.47	
45 to 135	1.5 to 3.0	2.330	2.653	1.208	0.862	0.157	-0.603	0.032	65	3.53 ± 0.48
	3.0 to 4.5	3.783	2.665	1.200	0.860	-0.041	-0.636	0.036	110	4.11 ± 0.43
	4.5 to 6.0	5.321	2.663	1.198	0.860	0.023	-0.672	0.043	160	3.82 ± 0.34
	6.0 to 7.5	6.755	2.656	1.204	0.861	0.059	-0.653	0.052	170	3.14 ± 0.26
	7.5 to 9.0	8.293	2.660	1.200	0.860	0.023	-0.624	0.064	190	2.80 ± 0.22
	9.0 to 10.5	9.716	2.659	1.199	0.860	0.022	-0.681	0.077	180	2.37 ± 0.19
	10.5 to 12.0	11.121	2.658	1.197	0.860	0.039	-0.637	0.092	180	2.44 ± 0.19
	12.0 to 13.5	12.741	2.680	1.195	0.855	0.007	-0.639	0.112	130	1.76 ± 0.16
	13.5 to 15.0	14.145	2.685	1.197	0.854	-0.025	-0.611	0.133	91	1.28 ± 0.14
	15.0 to 16.5	15.686	2.701	1.180	0.850	-0.026	-0.631	0.156	71	1.18 ± 0.14
16.5 to 18.0	17.202	2.770	1.144	0.834	-0.164	-0.577	0.187	42	1.07 ± 0.17	
135 to 225	1.5 to 3.0	2.242	2.705	1.171	0.852	-0.893	0.613	0.028	59	3.00 ± 0.46
	3.0 to 4.5	3.832	2.742	1.160	0.844	-0.902	0.643	0.032	75	2.59 ± 0.34
	4.5 to 6.0	5.247	2.766	1.145	0.839	-0.886	0.587	0.037	110	3.11 ± 0.32
	6.0 to 7.5	6.670	2.810	1.125	0.828	-0.910	0.673	0.046	100	2.60 ± 0.27
	7.5 to 9.0	8.280	2.839	1.096	0.822	-0.891	0.603	0.058	99	1.90 ± 0.20
	9.0 to 10.5	9.633	2.871	1.088	0.814	-0.885	0.587	0.072	70	1.34 ± 0.16
	10.5 to 12.0	11.237	2.905	1.059	0.805	-0.894	0.613	0.092	64	1.37 ± 0.18
	12.0 to 13.5	12.680	2.920	1.051	0.802	-0.870	0.523	0.113	41	1.09 ± 0.18
13.5 to 15.0	14.108	2.945	1.044	0.794	-0.841	0.431	0.137	26	0.86 ± 0.17	

TABLE I (Continued)

ϕ (deg)	Bin		Kinematic averages							Result
	θ (deg)	θ (deg)	W (GeV)	$-k^2$ (GeV ²)	ϵ	$\cos\phi$	$\cos 2\phi$	$-t$ (GeV ²)	N	$\frac{d\sigma}{d\Omega_{\pi}} \left(\frac{\mu b}{sr} \right)$
(d) Data point 4										
all	≤ 1.5	0.963	2.455	1.314	0.896	-0.074	-0.107	0.047	51	3.63 ± 0.56
-135 to -45	1.5 to 3.0	2.427	2.461	1.301	0.896	-0.228	-0.551	0.048	31	3.86 ± 0.75
	3.0 to 4.5	3.773	2.470	1.330	0.893	-0.168	-0.676	0.053	34	3.38 ± 0.62
	4.5 to 6.0	5.205	2.468	1.310	0.894	-0.140	-0.693	0.057	30	3.02 ± 0.58
	6.0 to 7.5	6.623	2.496	1.291	0.890	-0.275	-0.591	0.061	25	3.44 ± 0.74
-45 to 45	1.5 to 3.0	2.278	2.401	1.355	0.903	0.880	0.565	0.056	21	3.88 ± 0.92
	3.0 to 4.5	3.789	2.381	1.366	0.906	0.892	0.609	0.063	32	3.60 ± 0.68
	4.5 to 6.0	5.246	2.363	1.379	0.908	0.913	0.680	0.070	24	4.08 ± 0.90
	6.0 to 7.5	6.848	2.327	1.390	0.913	0.893	0.609	0.083	21	6.01 ± 1.50
45 to 135	1.5 to 3.0	2.226	2.451	1.325	0.896	-0.084	-0.734	0.050	31	3.51 ± 0.68
	3.0 to 4.5	3.898	2.450	1.322	0.897	0.007	-0.619	0.055	57	4.15 ± 0.61
	4.5 to 6.0	5.305	2.461	1.316	0.895	-0.083	-0.718	0.059	74	3.49 ± 0.44
	6.0 to 7.5	6.757	2.477	1.298	0.893	-0.178	-0.603	0.065	81	3.20 ± 0.38
	7.5 to 9.0	8.221	2.473	1.303	0.893	-0.132	-0.642	0.075	88	2.63 ± 0.30
	9.0 to 10.5	9.652	2.486	1.303	0.891	-0.163	-0.694	0.086	99	3.00 ± 0.32
	10.5 to 12.0	11.168	2.491	1.301	0.890	-0.138	-0.681	0.101	70	1.96 ± 0.25
	12.0 to 13.5	12.697	2.503	1.285	0.888	-0.187	-0.656	0.117	54	1.32 ± 0.23
	13.5 to 15.0	14.328	2.571	1.246	0.878	-0.373	-0.594	0.134	43	1.58 ± 0.24
	15.0 to 16.5	15.630	2.604	1.234	0.872	-0.424	-0.541	0.153	43	2.17 ± 0.34
16.5 to 18.0	17.208	2.657	1.199	0.862	-0.519	-0.424	0.180	20	1.24 ± 0.28	
135 to 225	1.5 to 3.0	2.341	2.491	1.289	0.891	-0.916	0.693	0.044	32	2.89 ± 0.54
	3.0 to 4.5	3.780	2.519	1.287	0.886	-0.899	0.630	0.047	66	3.05 ± 0.41
	4.5 to 6.0	5.216	2.555	1.258	0.881	-0.900	0.634	0.050	74	2.51 ± 0.30
	6.0 to 7.5	6.735	2.574	1.246	0.878	-0.915	0.689	0.057	94	2.59 ± 0.28
	7.5 to 9.0	8.220	2.604	1.232	0.872	-0.901	0.639	0.066	100	2.29 ± 0.24
	9.0 to 10.5	9.687	2.635	1.208	0.867	-0.909	0.669	0.077	83	1.58 ± 0.18
	10.5 to 12.0	11.249	2.674	1.193	0.859	-0.916	0.693	0.093	94	1.70 ± 0.18
	12.0 to 13.5	12.761	2.692	1.187	0.855	-0.894	0.611	0.112	67	1.13 ± 0.14
	13.5 to 15.0	14.290	2.733	1.167	0.847	-0.904	0.650	0.134	73	1.12 ± 0.14
	15.0 to 16.5	15.777	2.775	1.139	0.837	-0.928	0.733	0.159	56	0.78 ± 0.11
	16.5 to 18.0	17.063	2.799	1.130	0.832	-0.924	0.717	0.183	35	0.50 ± 0.09
	18.0 to 19.5	18.743	2.833	1.114	0.824	-0.905	0.654	0.220	26	0.36 ± 0.07
	19.5 to 21.0	20.186	2.856	1.092	0.818	-0.896	0.623	0.253	26	0.37 ± 0.07
21.0 to 22.5	21.636	2.885	1.077	0.811	-0.881	0.596	0.292	22	0.33 ± 0.07	
(e) Data point 5										
135 to 225	12.0 to 13.5	12.691	2.417	1.346	0.901	-0.930	0.746	0.120	33	1.63 ± 0.29
	13.5 to 15.0	14.278	2.438	1.322	0.898	-0.919	0.699	0.137	37	1.03 ± 0.17
	15.0 to 16.5	15.687	2.465	1.306	0.895	-0.934	0.759	0.154	39	0.90 ± 0.15
	16.5 to 18.0	17.161	2.491	1.295	0.891	-0.938	0.774	0.175	44	0.75 ± 0.12
	18.0 to 19.5	18.719	2.504	1.286	0.889	-0.899	0.635	0.200	61	0.99 ± 0.13
	19.5 to 21.0	20.269	2.541	1.272	0.883	-0.924	0.718	0.230	45	0.70 ± 0.10
	21.0 to 22.5	21.671	2.580	1.255	0.877	-0.936	0.763	0.260	32	0.48 ± 0.08
	22.5 to 24.0	23.271	2.612	1.227	0.871	-0.931	0.741	0.295	22	0.33 ± 0.07
	24.0 to 25.5	24.667	2.648	1.219	0.864	-0.950	0.813	0.334	26	0.36 ± 0.07
	25.5 to 27.0	26.259	2.669	1.193	0.861	-0.904	0.644	0.376	21	0.29 ± 0.07

TABLE I (Continued)

Bin		Kinematic averages							Result	
ϕ (deg)	θ (deg)	θ (deg)	W (GeV)	$-k^2$ (GeV ²)	ϵ	$\cos\phi$	$\cos 2\phi$	$-t$ (GeV ²)	N	$\frac{d\sigma}{d\Omega_\pi} \left(\frac{\mu\text{b}}{\text{sr}} \right)$
(f) Data point 6										
all	≤ 1.5	1.032	2.146	1.187	0.942	-0.052	0.062	0.067	78	4.54 ± 0.59
-135 to -45	1.5 to 3.0	2.204	2.144	1.192	0.942	-0.012	-0.543	0.068	40	4.11 ± 0.76
	3.0 to 4.5	3.735	2.143	1.191	0.942	0.097	-0.648	0.071	65	4.07 ± 0.57
	4.5 to 6.0	5.190	2.160	1.187	0.940	-0.108	-0.593	0.074	64	3.74 ± 0.53
	6.0 to 7.5	6.704	2.130	1.190	0.943	0.152	-0.635	0.083	54	2.98 ± 0.46
	7.5 to 9.0	8.178	2.154	1.194	0.940	0.022	-0.587	0.087	62	4.20 ± 0.61
	9.0 to 10.5	9.654	2.122	1.204	0.943	0.211	-0.521	0.101	31	2.91 ± 0.59
-45 to 45	1.5 to 3.0	2.415	2.108	1.216	0.944	0.888	0.593	0.075	76	5.82 ± 0.80
	3.0 to 4.5	3.784	2.084	1.205	0.947	0.910	0.670	0.080	88	3.88 ± 0.47
	4.5 to 6.0	5.289	2.065	1.225	0.948	0.898	0.628	0.089	150	5.14 ± 0.49
	6.0 to 7.5	6.764	2.041	1.228	0.950	0.915	0.689	0.098	140	3.98 ± 0.38
	7.5 to 9.0	8.156	2.023	1.231	0.952	0.893	0.609	0.107	150	4.01 ± 0.37
	9.0 to 10.5	9.750	1.999	1.245	0.953	0.908	0.665	0.120	170	3.47 ± 0.30
	10.5 to 12.0	11.220	1.978	1.249	0.955	0.909	0.667	0.132	150	2.95 ± 0.27
	12.0 to 13.5	12.735	1.949	1.258	0.957	0.934	0.757	0.148	130	2.61 ± 0.26
	13.5 to 15.0	14.191	1.930	1.267	0.958	0.926	0.728	0.163	140	2.95 ± 0.28
	15.0 to 16.5	15.741	1.905	1.277	0.959	0.935	0.760	0.181	130	2.60 ± 0.25
	16.5 to 18.0	17.201	1.885	1.290	0.960	0.945	0.795	0.198	130	2.61 ± 0.26
	18.0 to 19.5	18.800	1.865	1.292	0.962	0.943	0.787	0.216	79	1.89 ± 0.24
	19.5 to 21.0	20.205	1.844	1.309	0.963	0.955	0.831	0.236	64	1.60 ± 0.22
21.0 to 22.5	21.721	1.820	1.321	0.964	0.976	0.909	0.257	41	1.36 ± 0.22	
45 to 135	1.5 to 3.0	2.293	2.140	1.211	0.942	0.005	-0.628	0.070	61	3.87 ± 0.56
	3.0 to 4.5	3.758	2.142	1.192	0.942	0.097	-0.633	0.071	110	3.64 ± 0.41
	4.5 to 6.0	5.280	2.144	1.192	0.942	0.011	-0.622	0.076	160	4.30 ± 0.40
	6.0 to 7.5	6.756	2.152	1.201	0.940	-0.011	0.619	0.082	190	4.00 ± 0.33
	7.5 to 9.0	8.294	2.150	1.189	0.941	0.005	-0.656	0.089	190	3.61 ± 0.29
	9.0 to 10.5	9.695	2.159	1.193	0.940	-0.033	-0.618	0.097	180	3.64 ± 0.30
	10.5 to 12.0	11.205	2.168	1.189	0.939	-0.064	-0.609	0.107	160	2.76 ± 0.24
	12.0 to 13.5	12.729	2.173	1.187	0.938	-0.064	-0.602	0.119	140	2.59 ± 0.24
	13.5 to 15.0	14.119	2.181	1.185	0.937	-0.078	-0.596	0.131	130	2.60 ± 0.25
	15.0 to 16.5	15.682	2.193	1.182	0.936	-0.097	-0.534	0.146	110	2.77 ± 0.29
	16.5 to 18.0	17.171	2.228	1.175	0.932	-0.173	-0.540	0.163	67	2.07 ± 0.27
	18.0 to 19.5	18.719	2.275	1.154	0.927	-0.277	-0.491	0.181	45	2.08 ± 0.33
	19.5 to 21.0	20.133	2.344	1.126	0.919	-0.417	-0.388	0.200	20	1.29 ± 0.29
135 to 225	1.5 to 3.0	2.252	2.175	1.186	0.939	-0.901	0.639	0.064	49	3.78 ± 0.61
	3.0 to 4.5	3.820	2.205	1.187	0.935	-0.906	0.656	0.064	83	4.15 ± 0.52
	4.5 to 6.0	5.269	2.230	1.159	0.934	-0.904	0.648	0.064	110	4.18 ± 0.45
	6.0 to 7.5	6.779	2.258	1.157	0.930	-0.899	0.631	0.068	120	3.12 ± 0.32
	7.5 to 9.0	8.268	2.277	1.143	0.929	-0.899	0.632	0.074	130	3.29 ± 0.32
	9.0 to 10.5	9.749	2.307	1.145	0.925	-0.889	0.597	0.082	120	2.33 ± 0.24
	10.5 to 12.0	11.156	2.334	1.122	0.922	-0.913	0.680	0.091	140	2.75 ± 0.26
	12.0 to 13.5	12.757	2.360	1.112	0.919	-0.902	0.643	0.104	110	1.91 ± 0.20
	13.5 to 15.0	14.172	2.379	1.109	0.916	-0.890	0.602	0.119	110	1.86 ± 0.18
	15.0 to 16.5	15.814	2.412	1.093	0.912	-0.901	0.640	0.138	100	1.57 ± 0.16
	16.5 to 18.0	17.175	2.439	1.083	0.908	-0.891	0.605	0.157	61	0.90 ± 0.12
	18.0 to 19.5	18.786	2.463	1.069	0.905	-0.884	0.579	0.180	65	0.98 ± 0.12
	19.5 to 21.0	20.331	2.508	1.049	0.898	-0.933	0.749	0.209	30	0.46 ± 0.10
	21.0 to 22.5	21.711	2.519	1.041	0.897	-0.868	0.522	0.235	33	0.67 ± 0.12
	22.5 to 24.0	23.221	2.542	1.057	0.892	-0.833	0.401	0.269	27	0.60 ± 0.12

TABLE I (Continued)

Bin		Kinematic averages							Result	
ϕ (deg)	θ (deg)	θ (deg)	W (GeV)	$-k^2$ (GeV ²)	ϵ	$\cos\phi$	$\cos 2\phi$	$-t$ (GeV ²)	N	$\frac{d\sigma}{d\Omega_\pi} \left(\frac{\mu\text{b}}{\text{sr}} \right)$
(g) Data point 7										
all	≤ 1.5	1.026	2.664	2.000	0.819	0.028	0.016	0.067	36	1.78 ± 0.32
-135 to -45	1.5 to 3.0	2.285	2.654	2.006	0.823	0.201	-0.664	0.070	16	1.38 ± 0.36
	3.0 to 4.5	3.714	2.655	2.017	0.822	0.074	-0.614	0.077	28	1.91 ± 0.39
	4.5 to 6.0	5.250	2.663	2.005	0.820	0.036	-0.582	0.085	33	2.00 ± 0.37
	6.0 to 7.5	6.611	2.653	2.015	0.822	0.127	-0.447	0.096	20	1.49 ± 0.35
-45 to 45	1.5 to 3.0	2.308	2.613	2.054	0.830	0.923	0.714	0.078	18	1.42 ± 0.35
	3.0 to 4.5	3.863	2.592	2.059	0.835	0.933	0.751	0.086	38	1.62 ± 0.28
	4.5 to 6.0	5.232	2.562	2.107	0.840	0.904	0.650	0.101	44	1.63 ± 0.27
	6.0 to 7.5	6.667	2.540	2.115	0.844	0.888	0.594	0.112	49	1.65 ± 0.26
	7.5 to 9.0	8.217	2.512	2.145	0.849	0.897	0.624	0.130	54	1.57 ± 0.24
	9.0 to 10.5	9.586	2.490	2.158	0.852	0.918	0.697	0.146	45	1.21 ± 0.19
	10.5 to 12.0	11.251	2.460	2.193	0.856	0.889	0.595	0.170	43	1.37 ± 0.22
12.0 to 13.5	12.771	2.446	2.192	0.859	0.902	0.640	0.191	28	1.01 ± 0.21	
45 to 135	1.5 to 3.0	2.313	2.663	2.015	0.821	-0.034	-0.684	0.071	20	1.71 ± 0.42
	3.0 to 4.5	3.917	2.655	2.011	0.822	0.000	-0.601	0.077	40	1.68 ± 0.29
	4.5 to 6.0	5.298	2.669	1.995	0.820	0.023	-0.654	0.084	43	1.36 ± 0.22
	6.0 to 7.5	6.834	2.682	1.987	0.816	-0.048	-0.610	0.093	61	1.66 ± 0.23
	7.5 to 9.0	8.352	2.664	1.998	0.820	0.026	-0.686	0.108	51	1.09 ± 0.16
	9.0 to 10.5	9.775	2.667	1.980	0.820	0.002	-0.649	0.122	71	1.22 ± 0.16
	10.5 to 12.0	11.169	2.649	2.019	0.822	0.054	-0.667	0.143	57	0.98 ± 0.14
	12.0 to 13.5	12.697	2.670	2.002	0.818	0.020	-0.662	0.160	54	0.84 ± 0.12
	13.5 to 15.0	14.230	2.688	1.985	0.813	-0.034	-0.679	0.185	54	0.84 ± 0.12
	15.0 to 16.5	15.630	2.682	1.995	0.814	-0.021	-0.686	0.208	37	0.62 ± 0.11
16.5 to 18.0	17.184	2.694	1.973	0.810	-0.019	-0.588	0.238	28	0.55 ± 0.11	
135 to 225	1.5 to 3.0	2.236	2.703	2.015	0.811	-0.916	0.692	0.067	16	1.39 ± 0.36
	3.0 to 4.5	3.828	2.746	1.941	0.802	-0.895	0.616	0.067	38	1.65 ± 0.30
	4.5 to 6.0	5.238	2.767	1.920	0.797	-0.913	0.684	0.070	31	1.21 ± 0.23
	6.0 to 7.5	6.720	2.796	1.855	0.792	-0.902	0.641	0.077	44	1.27 ± 0.20
	7.5 to 9.0	8.182	2.829	1.854	0.783	-0.924	0.720	0.089	41	1.04 ± 0.17
	9.0 to 10.5	9.717	2.862	1.816	0.775	-0.902	0.641	0.103	42	0.99 ± 0.16
	10.5 to 12.0	11.399	2.907	1.778	0.763	-0.908	0.661	0.125	25	0.59 ± 0.12
	12.0 to 13.5	12.777	2.899	1.811	0.764	-0.872	0.538	0.149	23	0.58 ± 0.13

The virtual-photoproduction cross section has the form

$$\frac{d\sigma}{d\Omega_\pi} = A + \epsilon B \cos 2\phi + \epsilon C + \left\{ \frac{1}{2} [\epsilon(1 + \epsilon)] \right\}^{1/2} D \cos \phi. \quad (3)$$

ϵ is the virtual-photon polarization parameter. A , B , C , and D are functions of k^2 , W , and θ and refer, respectively, to unpolarized transverse production, interference between the two transverse helicity states, purely scalar production, and scalar-transverse interference.

A Monte Carlo calculation was made assuming unit center-of-mass cross section and incorporating all multiple scattering and detector resolution effects. This enabled us to correct the number of events in each bin for the acceptance of the ap-

paratus, and hence calculate the observed cross section for each bin. The normalization of the experiment was checked by independently observing elastically scattered electrons in both spectrometers and comparing the observed cross sections with the accepted elastic-scattering cross sections. The Monte Carlo program gave an angular resolution of about 0.3° full width in the center-of-mass system and indicated that the resolution in angle and energy was multiple-scattering-dominated.

The measured cross sections were corrected for nuclear absorption, dead-time effects, target-wall background, and pion decay. The sum of all these corrections was less than 15% at all data points.

The cross sections were also corrected for losses due to the radiation of soft photons. The

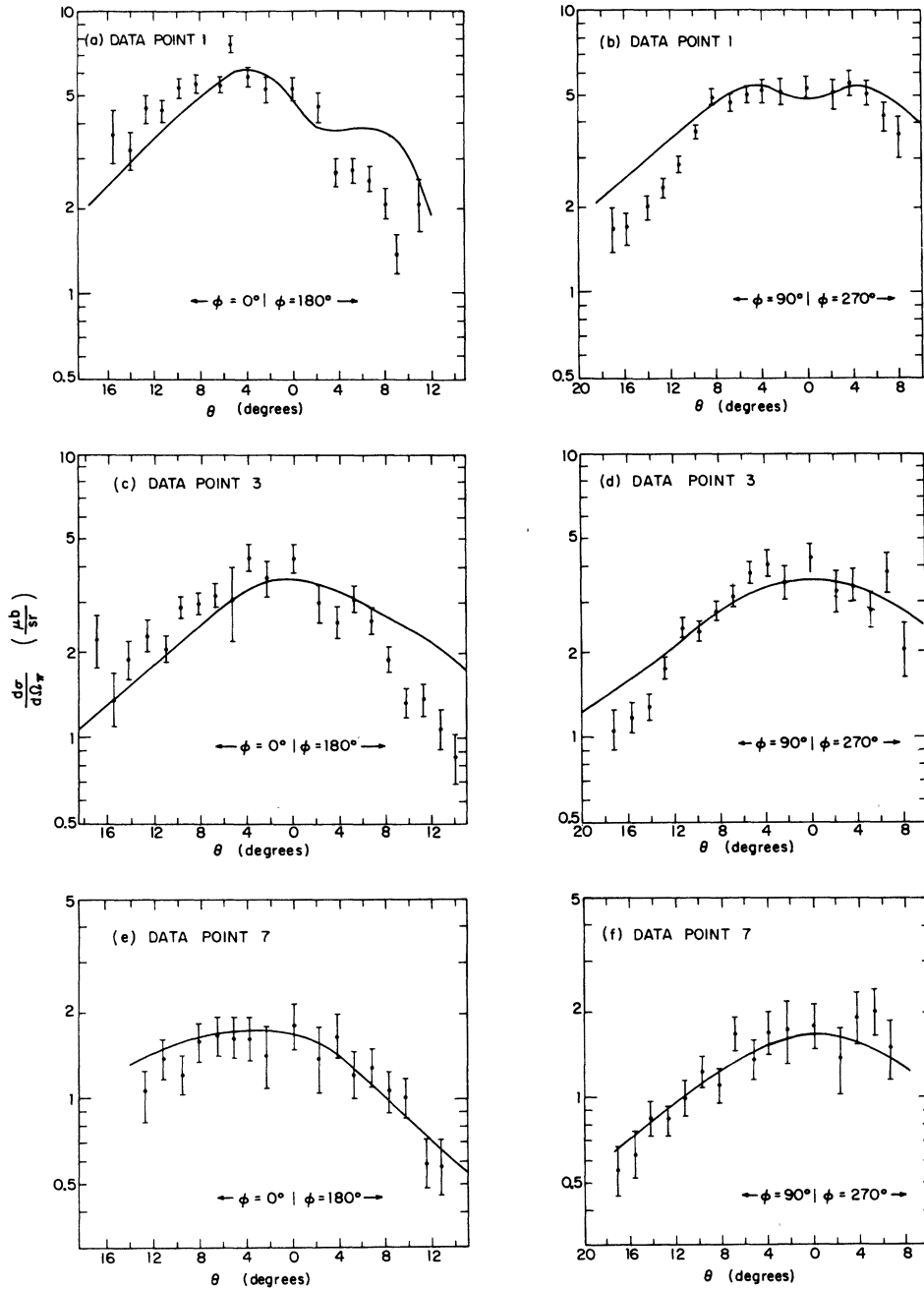


FIG. 4. A plot of the virtual-photoproduction cross sections versus θ for data points 1, 3, and 7. The solid curves are the predictions of Berends's theory.

- (a) $W = 2.67$, $-k^2 = 0.62$, $\phi = 0^\circ$, 180° ; (b) $W = 2.67$, $-k^2 = 0.62$, $\phi = 90^\circ$, 270° ; (c) $W = 2.66$, $-k^2 = 1.2$, $\phi = 0^\circ$, 180° ;
 (d) $W = 2.66$, $-k^2 = 1.2$, $\phi = 90^\circ$, 270° ; (e) $W = 2.66$, $-k^2 = 2.0$, $\phi = 0^\circ$, 180° ; (f) $W = 2.66$, $-k^2 = 2.0$, $\phi = 90^\circ$, 270° .

prescription for the radiative correction was taken from the work of Bartl and Urban.⁷ It was checked by an independent calculation based on the work of Meister and Yennie.⁸ The two calculations agreed to better than 0.5% for the data presented here. The full radiative correction was roughly

30% for all the data points.

The errors on the cross sections presented in this paper are statistical only. There is an additional systematic uncertainty which is estimated to be less than 7%. This quoted systematic uncertainty is based on the normalization check with

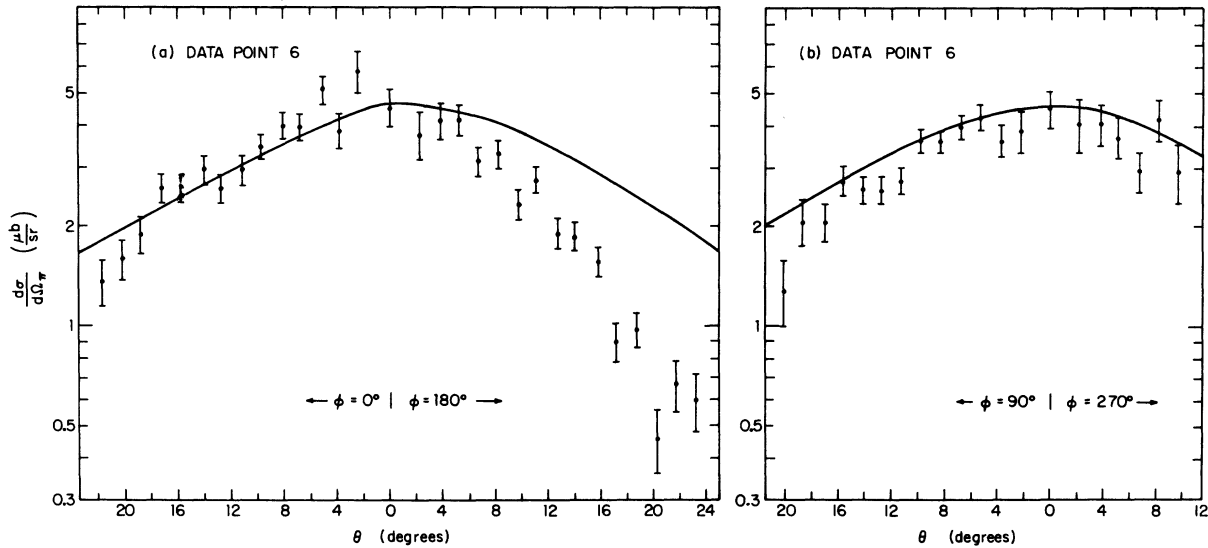


FIG. 5. A plot of the virtual-photoproduction cross section versus θ for data point 6. The solid curves are the predictions of Berends's theory.

(a) $W = 2.15$, $-k^2 = 1.19$, $\phi = 0^\circ, 180^\circ$; (b) $W = 2.15$, $-k^2 = 1.19$, $\phi = 90^\circ, 270^\circ$.

the electron-scattering measurements and the uncertainty in the corrections to the data.

III. RESULTS

Tables I(a) through I(g) list the cross sections measured in this experiment. Owing to the high

correlation of the average virtual-photon parameters with the observed angle between the pion and the virtual-photon direction, the average values of the virtual-photon parameters over the events in a bin are also included for each bin.

The results are shown graphically in Figs. 4 through 8 as a function of the polar angle θ of the

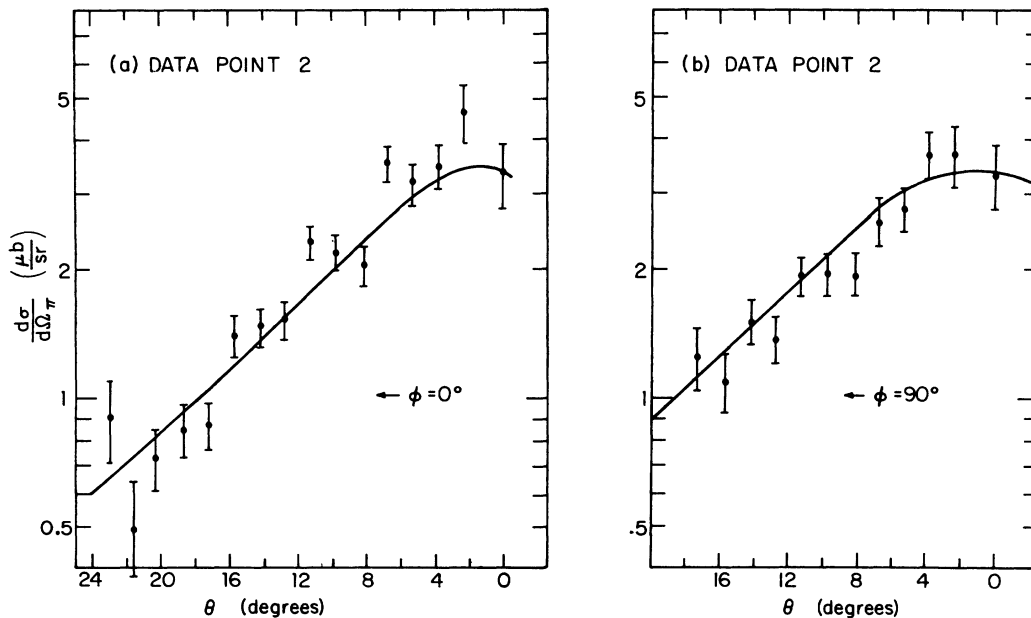


FIG. 6. A plot of the virtual-photoproduction cross section versus θ for data point 2. The solid curves are the predictions of Berends's theory.

(a) $W = 2.90$, $-k^2 = 1.07$, $\phi = 0^\circ$; (b) $W = 2.90$, $-k^2 = 1.07$, $\phi = 90^\circ$.

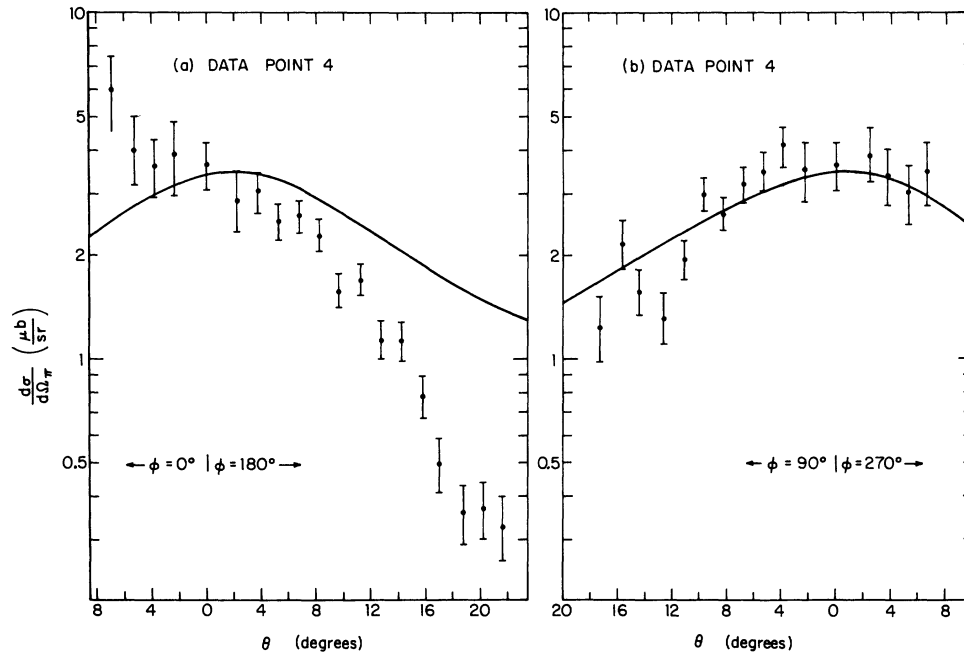


FIG. 7. A plot of the virtual-photoproduction cross section versus θ for data point 4. The solid curves are the predictions of Berends's theory.

(a) $W = 2.46$, $-k^2 = 1.31$, $\phi = 0^\circ$, 180° ; (b) $W = 2.46$, $-k^2 = 1.31$, $\phi = 90^\circ$, 270° .

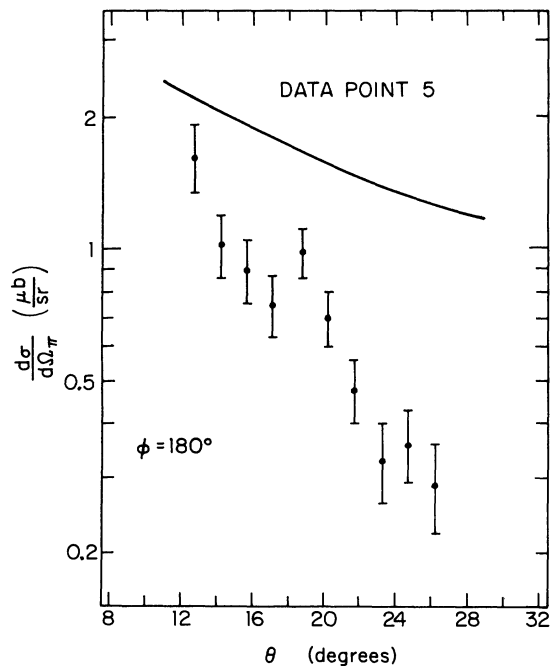


FIG. 8. A plot of the virtual-photoproduction cross section versus θ for data point 5. The solid curve is the prediction of Berends's theory. $W \approx 2.50$, $-k^2 \approx 1.30$, $\phi = 180^\circ$.

emitted pion for the virtual-photoproduction plane parallel to the electron-scattering plane ($\phi = 0^\circ$ or 180°) and for the virtual-photoproduction plane perpendicular to the electron-scattering plane ($\phi = -90^\circ$ or 90°). The values of W , $-k^2$, and ϵ listed for each curve are the average values for the central bin. The values of W , $-k^2$, and ϵ change considerably as θ changes, and this change must be taken into account if the data are compared with theory or used to separate out the interference terms B and D .

We shall now compare the measured cross sections with the electric Born model with dispersion-theory corrections as developed by Berends.⁶ Before we can calculate the predicted angular distributions, we must arrive at a value for the pion form factor, the only free parameter in the theory. At zero degrees the interference terms B and D vanish and the theory predicts that the pion-exchange diagram dominates the cross section. For these reasons we choose a value for the pion form factor by fitting the data in the five central bins ($\theta_{\text{c.m.}} \leq 3^\circ$) at each data point. Table II summarizes the values of $F_\pi(-k^2)$ determined using this procedure. Figure 9 shows graphically the values of the pion form factor determined from this experiment and earlier experiments at the CEA,^{1,2} DESY³ and NINA.⁴

TABLE II. Values of the pion form factor $F_{\pi}(-k^2)$ determined from this experiment using the data for $\theta_{c.m.} \leq 3^\circ$. Uncertainties are statistical only.

Data point	$-k^2$ (GeV ²)	$F_{\pi}(-k^2)$
1	0.620	0.465 ± 0.015
2	1.069	0.332 ± 0.017
3	1.204	0.291 ± 0.010
4	1.314	0.266 ± 0.013
6	1.200	0.288 ± 0.012
7	2.015	0.185 ± 0.011

A functional parametrization of the pion form factor was then obtained by making a fit to these measurements together with the previous measurements made at the CEA. A simple polynomial gave a satisfactory fit to the eleven data points. The form obtained was

$$F_{\pi}(-k^2) = 1 - 1.577(-k^2) + 1.635(-k^2)^2 - 0.909(-k^2)^3 + 0.192(-k^2)^4.$$

Other functional forms suggested by quark models of the electron-pion interaction also fit the data quite adequately.⁹

The prediction of the theory assuming the polynomial form for $F_{\pi}(-k^2)$ was then calculated for each bin using the average value of the kinematic parameters for that bin. The smooth curves shown in Figs. 4 through 8 give the theoretical predictions. The actual value calculated for each bin deviated by a very small amount from the smooth curve due to the statistical nature of the average bin parameters. The theory does not fit the data at large angles and does not describe correctly the scalar-transverse interference term. Nevertheless, the agreement at small angles between theory and experiment does not deteriorate as $-k^2$ increases at fixed W .

There is a high degree of correlation between the kinematic parameters; the correlation is so complete that it is possible to interpolate in one variable (W) the data from data points 2, 3, 4, and 5 and obtain $\phi = 0^\circ$ and $\phi = 180^\circ$ cross sections at fixed W , $-k^2$, and ϵ . Table III summarizes the interpolated cross sections for 3 nonoverlapping sets of virtual-photon parameters. A linear interpolation between adjacent points was used to determine the interpolated cross sections. Figure 10 shows the interpolated cross sections together with the predictions of the theory.

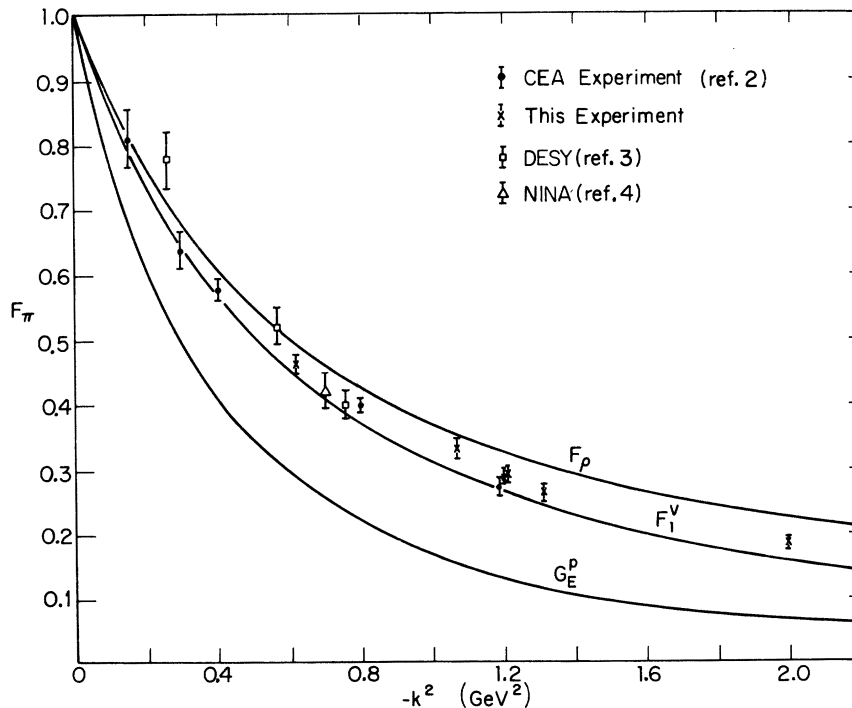


FIG. 9. A plot versus $-k^2$ of the pion form factor as determined from this experiment and earlier experiments at CEA, DESY, and NINA. Also shown for comparison are three form factors: F_{ρ} , a simple ρ -pole form factor; F_1^V , the Dirac isovector part of the nucleon form factor; and G_E^p , the electric form factor of the proton.

TABLE III. The interpolated cross sections determined from data points 2, 3, 4, and 5. Uncertainties are statistical only.

Bin		$\frac{d\sigma}{d\Omega_\pi} \left(\frac{\mu\text{b}}{\text{sr}} \right)$		
ϕ (deg)	θ (deg)	$W=2.55, -k^2=1.26,$ and $\epsilon=0.88$	$W=2.66, -k^2=1.20,$ and $\epsilon=0.86$	$W=2.75, -k^2=1.16,$ and $\epsilon=0.84$
-45 to 45	15.75	1.41 ± 0.15		
	14.25	1.55 ± 0.18		
	12.75	1.76 ± 0.20		
	11.25	2.19 ± 0.22	2.31 ± 0.21	
	9.75	2.63 ± 0.24	2.28 ± 0.22	
	8.25	2.75 ± 0.25	2.32 ± 0.23	2.05 ± 0.22
	6.75	3.23 ± 0.30	3.38 ± 0.32	3.52 ± 0.33
	5.25	3.08 ± 0.30	3.12 ± 0.32	3.15 ± 0.34
	3.75	4.25 ± 0.49	4.08 ± 0.44	3.78 ± 0.43
	2.25	3.73 ± 0.64	3.87 ± 0.56	4.20 ± 0.62
all ϕ	0.0	3.95 ± 0.53	4.32 ± 0.50	3.94 ± 0.52
135 to 225	2.25	2.92 ± 0.52	2.98 ± 0.48	3.00 ± 0.46
	3.75	2.99 ± 0.40	2.76 ± 0.37	2.59 ± 0.34
	5.25	2.51 ± 0.30	2.81 ± 0.31	3.11 ± 0.32
	6.75		2.59 ± 0.28	2.60 ± 0.27
	8.25		2.20 ± 0.23	2.05 ± 0.22
	9.75		1.58 ± 0.18	1.46 ± 0.17
	11.25		1.70 ± 0.18	1.59 ± 0.18
	12.75		1.19 ± 0.16	1.12 ± 0.15
	14.25		1.10 ± 0.15	1.12 ± 0.14
	15.75		0.82 ± 0.12	0.78 ± 0.11
	17.25		0.61 ± 0.10	
	18.75		0.69 ± 0.10	
	20.25		0.58 ± 0.09	
	21.75		0.44 ± 0.08	
23.25		0.33 ± 0.07		
24.75		0.36 ± 0.07		
26.25		0.29 ± 0.07		

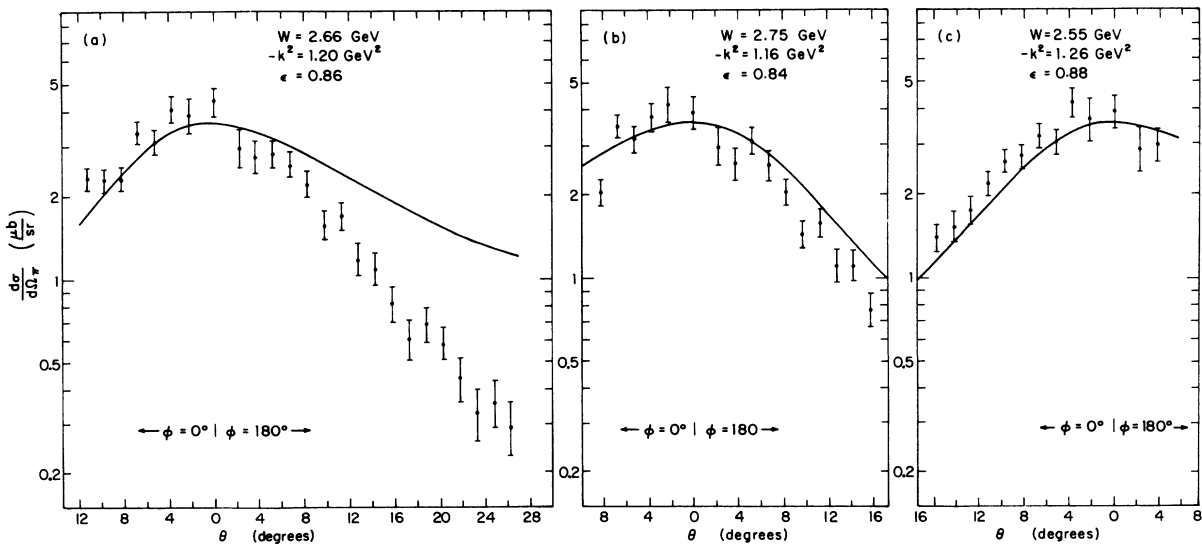


FIG. 10. A plot of the interpolated cross section determined from data points 2, 3, 4, and 5. The solid curves are the predictions of Berends's theory.

TABLE IV. The components of the cross section for $W=2.66$ GeV, $-k^2=1.2$ GeV², and $\epsilon=0.86$. Uncertainties are statistical only.

θ (deg)	$A + \epsilon C$ ($\mu\text{b}/\text{sr}$)	B ($\mu\text{b}/\text{sr}$)	D ($\mu\text{b}/\text{sr}$)
2.25	3.41 ± 0.26	0.02 ± 0.47	0.54 ± 0.45
3.75	3.60 ± 0.21	-0.33 ± 0.38	0.81 ± 0.36
5.25	3.14 ± 0.17	-0.33 ± 0.31	0.20 ± 0.27
6.75	3.24 ± 0.15	-0.47 ± 0.27	0.49 ± 0.26
8.25	2.35 ± 0.13	-0.16 ± 0.24	0.07 ± 0.20
9.75	2.15 ± 0.12	-0.20 ± 0.22	0.43 ± 0.16
11.25	2.22 ± 0.12	-0.20 ± 0.22	0.37 ± 0.16

The interpolated $\phi=0^\circ$ and $\phi=180^\circ$ cross sections at $W=2.66$, $-k^2=1.20$, $\epsilon=0.86$ can be combined with the $\phi=-90^\circ$ and $\phi=90^\circ$ data listed in Table I(c) which have the same values for these parameters. This makes possible a determination of the individual contributions $A + \epsilon C$, B , and D . Table IV summarizes the results of this analysis. Figure 11 shows these same results graphically, together with the predictions of the theory. This analysis shows that the theory does not describe correctly the scalar-transverse interference term.

IV. CONCLUSION

For small momentum transfers and all values of the virtual-photon mass $-k^2$, single-pion electroproduction can be adequately described by the electric Born model with dispersion-theory corrections. For fixed $-k^2$ the value of the pion form factor required to fit the data is independent of W and does not depend upon the minimum momentum transfer in the virtual photoproduction reaction. For the data points in this experiment with $-k^2=1.2$ GeV², the minimum momentum transfer and hence the minimum distance to the pion pole differs by almost a factor of two. The close agreement between the values of the pion form factor obtained at these two points indicates that the electric Born model gives a good representation of the data near the forward direction and gives credence to the value of the pion form factor obtained at higher $-k^2$. An alternate point of view is that this theory

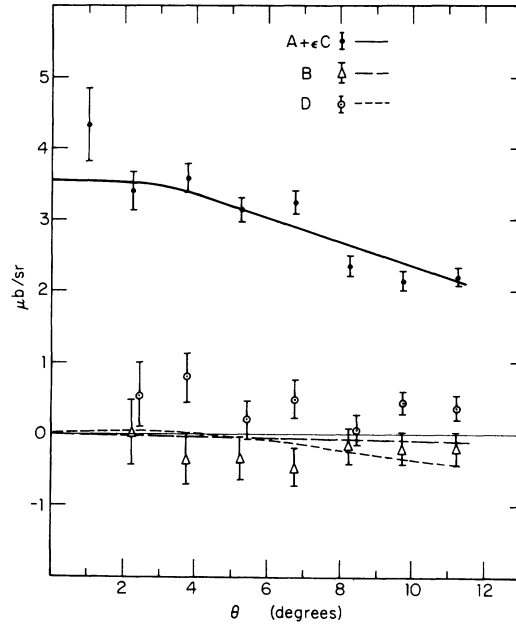


FIG. 11. A plot showing the separated components of the cross section, $A + \epsilon C$, B , and D , for $W=2.66$ GeV, $-k^2=1.2$ GeV², and $\epsilon=0.86$. The curves show the predictions of Berends's theory (see Ref. 6).

is providing us with a reasonable way of extrapolating the short distance to the pion pole to obtain the pion form factor as was first suggested by Frazer.¹⁰

The theory does not give an adequate representation of the scalar-transverse interference or of the data at large momentum transfer. The precision of the data warrants renewed theoretical attempts to understand fully this simplest of virtual-photon reactions.

ACKNOWLEDGMENTS

We would like to thank the Director, Professor Boyce McDaniel, and the staff of the Wilson Synchrotron for their gracious help during the course of this experiment. We also thank the staff of the Harvard Cyclotron Laboratory for assistance in construction of the apparatus. The program used for the electric Born model predictions was obtained from Professor F. Berends.

*Research supported in part by the U. S. Atomic Energy Commission and in part by the National Science Foundation.

†Present address: Physics Department, University of Rochester, Rochester, New York 14627.

¹C. N. Brown, C. R. Canizares, W. E. Cooper, A. M. Eisner, G. J. Feldman, C. A. Lichtenstein, L. Litt,

W. Lockeretz, V. B. Montana, and F. M. Pipkin, Phys. Rev. Lett. **26**, 987 (1971); **26**, 991 (1971).

²C. N. Brown, C. R. Canizares, W. E. Cooper, A. M. Eisner, G. J. Feldman, C. A. Lichtenstein, L. Litt, W. Lockeretz, V. B. Montana, and F. M. Pipkin, Phys. Rev. D **8**, 92 (1973).

³C. Driver, K. Heinloth, K. Hohne, G. Hofmann,

- P. Karow, D. Schmidt, G. Specht, and J. Rathje, *Phys. Lett.* **35B**, 77 (1971).
- ⁴P. S. Kummer, A. B. Clegg, F. Foster, G. Hughes, R. Siddle, J. Allison, B. Dickinson, E. Evangelides, M. Ibbotson, R. Lawson, R. S. Meaburn, H. E. Montgomery, W. J. Shuttleworth, and A. Sofair, *Nuovo Cimento Lett.* **1**, 1026 (1971); A. Sofair, J. Allison, B. Dickinson, E. Evangelides, M. Ibbotson, R. Lawson, R. S. Meaburn, H. E. Montgomery, W. J. Shuttleworth, A. B. Clegg, F. Foster, G. Hughes, P. Kummer, and R. Siddle, *Nucl. Phys.* **B42**, 369 (1973).
- ⁵J. Engels, G. Schwiderski, and W. Schmidt, *Phys. Rev.* **166**, 1343 (1968).
- ⁶F. A. Berends, *Phys. Rev. D* **1**, 2590 (1970).
- ⁷A. Bartl and P. Urban, *Acta. Phys. Austriaca* **24**, 139 (1966).
- ⁸N. Meister and D. R. Yennie, *Phys. Rev.* **130**, 1210 (1963).
- ⁹R. Gatto and G. Preparata, DESY Report No. 73/15, 1973 (unpublished).
- ¹⁰W. R. Frazer, *Phys. Rev.* **115**, 1763 (1959).

PHYSICAL REVIEW D

VOLUME 9, NUMBER 5

1 MARCH 1974

Measurement of the K^0 coherent regeneration amplitude in Cu from 0.6 to 1.4 GeV/c

D. Birnbaum, * R. M. Edelstein, H. E. Fisk, † T. S. Roth, ‡
J. S. Russ, and R. C. Thatcher§
Carnegie-Mellon University, Pittsburgh, Pennsylvania 15213

E. W. Hoffman

Argonne National Laboratory, Argonne, Illinois 60439

(Received 4 September 1973)

The magnitude of $|f_{21}(0)|$, the coherent K^0 regeneration amplitude in Cu, has been measured for K momenta from 600 to 1400 MeV/c. Results are compared with predictions of an optical model using forward dispersion relation predictions for real parts of kaon-nucleon scattering amplitudes.

This paper reports a measurement of the momentum dependence of the K^0 coherent regeneration amplitude in copper through the Y^* resonance region from 600 to 1400 MeV/c. The experiment was performed in a 17.5° neutral beam at the Argonne Zero-Gradient Synchrotron (ZGS) and provides the most detailed study to date of the regeneration process in the low-momentum region.

The amplitude for coherent regeneration is

$$f_{21}(0) \equiv \frac{1}{2}[f(0) - \bar{f}(0)],$$

where $f(0)$ [$\bar{f}(0)$] is the $S=+1$ [$S=-1$] K -meson-nucleus forward scattering amplitude. Therefore, when either $f(0)$ or $\bar{f}(0)$ changes rapidly with momentum, e.g., near one of the Y^* resonance peaks, one might expect rather abrupt changes in $f_{21}(0)$. This experiment measures $|f_{21}(0)|$ by determining the number of coherently regenerated K_S^0 mesons decaying after a 12.7-cm-thick copper regenerator set into a K_L^0 beam.

The rate for producing $\pi^+\pi^-$ pairs is

$$R_{+-} = (K_L \text{ flux}) \frac{\Gamma_S(\pi^+\pi^-)}{\Gamma_S} \frac{(N\lambda\Lambda)^2}{\delta^2 + \frac{1}{4}} |f_{21}(0)|^2 f(\delta, L),$$

where

$$f(\delta, L) = (1 + e^{-l} - 2e^{-l/2} \cos \delta l) \exp(-N\sigma_T L),$$

$$\delta = |M_{K_L} - M_{K_S}| \tau_S,$$

L is the slab length, $\Lambda = \beta_K \gamma_K c \tau_S$, $l = L/\Lambda$, $\lambda = h/p_K$, $\Gamma_S(\pi^+\pi^-)/\Gamma_S$ is the K_S branching ratio to $\pi^+\pi^-$, N is the density of scattering centers, and σ_T is the K_L -nucleus total cross section. To determine $|f_{21}(0)|$, one must measure R_{+-} as a function of p_K , the K_L flux as a function of p_K , and σ_T . Everything else is known.

The experimental layout is shown in Fig. 1. The $\pi^+\pi^-$ pairs from K_S^0 decay are detected in a two-arm magnetic spectrometer. The large dipion opening angles at low momentum preclude using one large magnet. Each magnet had four magnetostrictive-readout wire spark chambers mounted upstream and four mounted downstream. Each chamber recorded X and Y coordinates. They were digitized using a Science Accessories readout system on-line to a PDP-7 computer. In each arm a threefold coincidence was formed from scintillation counters defining the entrance aperture of the magnet (L_1, R_1) and covering the exit of the spark chambers (L_2, L_3, R_2, R_3). Anticoincidence counters A_1, A_2, A_3 formed a box around the regenerator to veto events having charged parti-